SEMARAK ILMU PUBLISHING

CFD Letters

Journal homepage:
https://semarakilmu.com.my/journals/index.php/CFD_Letters/index
ISSN: 2180-1363

CFD Analysis into the Resistance Characteristics of Remotely Operated Vehicles When Submerges under Water and Sails on the Surface

Wasis Dwi Aryawan[1], I Ketut Aria Pria Utama[1,*], Yuda Apri Hermawan[1], Sutiyo[2]

[1] Department of Naval Architecture, Faculty of Marine Technology, Institut Teknologi Sepuluh Nopember (ITS), Surabaya 60111, Indonesia
[2] Department of Naval Architecture, Faculty of Engineering and Marine Sciences, Universitas Hang Tuah, Surabaya 60111, Indonesia

ARTICLE INFO

Article history:
Received 30 December 2022
Received in revised form 24 January 2023
Accepted 21 February 2023
Available online 1 August 2023

Keywords:
CFD; ROV; Resistance; Pressure; Free Surface; 100 m Depth

ABSTRACT

Remotely operated (underwater) vehicles, commonly known as ROVs, have a wide range of uses in the marine industry, including maintenance and repair. The research examines ROV pressure and resistance, is less likely at the present time. Furthermore, the design and operation of this remotely operated vehicle (ROV) rely heavily on accurate measurements of hydrodynamic loads. Computational Fluids Dynamic (CFD) technique makes it possible to obtain an accurate estimate of the forces that are being applied by the flow around the ROV hull. In this paper, an investigation of the resistance and pressure that the ROV experiences when on the surface and while submerged to a depth of 100 meters is presented. In addition, ROV was evaluated at several speeds, ranging from 0.5 to 1.5 metres per second. The speed of the ROV that is being evaluated will increase when significant impediments are introduced into the environment. This flips the direction of the pressure that is applied to the ROV hull. The CFD approach demonstrates the resistance that is generated on the ROV hull is, for the most part, affected by the speed at which it is moving. In free surface conditions, the average increase in resistance was 78.91%, and in submerged conditions, it was 74.24%. Nevertheless, the variation in test depth is where the main impact of the pressure value can be seen in the CFD simulation. Simulations conducted on the free surface indicate that the pressure on the ROV hull is about $1x10^{-3}$ kPa, whereas simulations conducted at a depth of 100 metres below the sea surface indicate that the pressure is approximately 972 kPa.

1. Introduction

The offshore energy sector has made great step in the use of ROV for subsea activities. Offshore renewable energy, oil and gas operations, and marine science are just a few of the fields that have conducted extensive studies into using remotely operated underwater vehicles for ship repair and maintenance [1]. Surveys are routinely performed to check on the condition of marine and offshore assets, and ROVs are a safe and cost-effective way to do this [2].

It is of the highest concern to build and design the robot or vessel in the most efficient and cost-effective way [3]. The pressure is increased with the depth of the water, which has a significant

* *Corresponding author.*
E-mail address: kutama@na.its.ac.id (I Ketut Aria Pria Utama)

https://doi.org/10.37934/cfdl.15.8.166178

impact on the underwater vehicle's stability. The vehicle's control system avoids instabilities (drag effects, ocean currents) and water composition [4]. The control independence could be restricted due to a number of factors, including the location and orientation of actuators on the vehicle, control surfaces, and the geometry of the ROV [5].

An ROV is basically a robot. A robot is different from its inanimate counterparts because it can move on its own. With the ability to move comes the ability to steer the robot, with increasing levels of autonomy, to reach a goal. Even though the ROV system is one of the simplest robotic designs and can be done with a variety of task navigation aids. Some ROV manufacturers are very enthusiastic about computer-based control models, which let users make their own control matrices.

This is an exciting new development in the field of subsea robotics. It will make it possible to create new techniques that are only limited by the user's creativity. This idea gives the user, not the design engineer (who may or may not understand the user's needs), control over the development of navigation features, which is the mission (who does understand the needs). It is important for the success of the product and, ultimately, the mission that systems are designed with the user in mind. This section talks about the main parts (Figure 1) of a typical ROV system and the tasks that ROVs do every day when situated underwater.

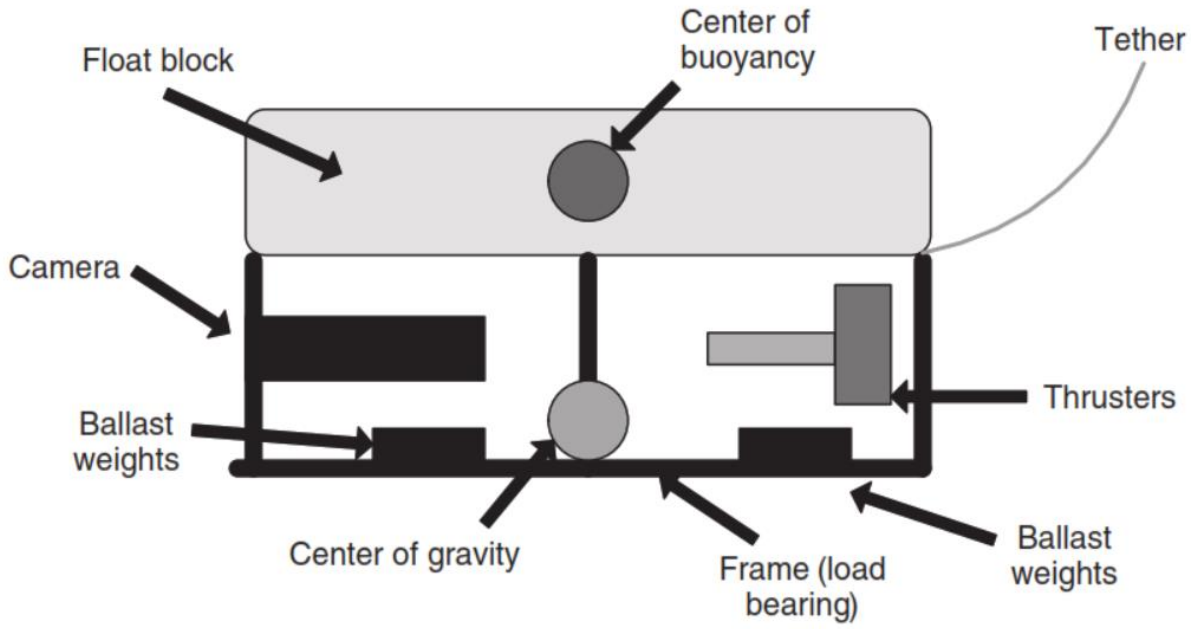

Fig. 1. ROV submersible components [6]

Every component of an ROV system needs to have a rating that corresponds to the greatest depth at which it can function in its respective underwater environment. On the other hand, there is no need for them to have an excessive amount of design. As the working depth increases and the ROV travels further into the ocean, the component wall thicknesses of the air-filled areas on the ROV will need to increase accordingly. Because of the increased wall thickness, the vehicle's overall weight increases, necessitating the installation of a more robust flotation system in order to accommodate the weight increase. This results in an increase in the amount of drag experienced owing to a greater cross-section, which necessitates an increase in the amount of power applied. The use of CFD is quite effective for predicting drag and lift on unmanned vehicles [7].

Since there is not much written information about how remotely operated vehicles (ROVs) work underwater, this paper is a first look at pressure and resistance in both free-surface and submerged

ROV operations. This research was conducted to determine and analyze the to acquire comprehensive information on resistance and pressure of ROV. Under conditions of a surface and a 100-meter depth below the water's surface, the ROV's performance settings are determined. In this paper, the effect of operating water depth on ROV resistance and pressure is determined using the CFD method. The ROV design concept was developed with the use of the Design Modeler; the next step is meshing, which is validated in accordance with the ITTC's criteria [8]. Furthermore, a visual representation of the ROV's obstructions and pressure is generated.

2. Methodology

2.1 CFD Governing Equation

The method of computational fluid dynamics, also known as CFD, was used to provide predictions about model resistance. In comparison to the findings of testing, the research on predicting the hull resistance of ship models with and without axe-bow modifications that was carried out by utilising CFD provided impressive results [9,10]. The computational fluid dynamics (CFD) model makes use of a three-dimensional equation that is derived from the Reynolds-averaged Navier-Stokes (RANS) equation. A stable incompressible flow, such as that provided by ANSYS-CFX, is used to successfully address the flow issues discovered in the ship's walls [11].

It has been discovered that the selection of turbulence models is critical in the modelling of wake fields. This research makes use of a turbulence model known SST (Shear Stress Transport) [12]. Numerous researchers have tested and validated k-ω SST model, and each one of them has come to the conclusion that the model produces accurate results [13-15]. For the purpose of solving the fluid flow field, the RANS solver that is included in ANSYS CFX is used. Eq. (1), Eq. (2), and Eq. (3) illustrate the continuity, RANS, and k-ω SST turbulence equations, respectively, as follows:

Continuity equation:

$$\frac{\partial \rho}{\partial t} + \frac{\partial}{\partial x_j}\left(\rho U_j\right) = 0 \tag{1}$$

where: ρ is define as fluid density, *t* for time, U_j for the flow velocity vector field.

RANS equation:

$$\rho \bar{f}_i + \frac{\partial}{\partial x_j}\left[-\bar{p}\delta_{ij} + \mu\left(\frac{\partial \bar{u}_i}{\partial x_j} + \frac{\partial \bar{u}_j}{\partial x_i}\right) - \overline{\rho u_i' u_j'}\right] - \rho \bar{u}_j \frac{\partial \bar{u}_i}{\partial x_j} = 0 \tag{2}$$

The mean momentum of a fluid element due to mean flow unsteadiness is shown on the left side of the RANS equation. That modification is compensated the mean body force ($\bar{f}$), the mean pressure field ($\bar{p}$), the viscous stress, $\mu\left(\frac{\partial \bar{u}_i}{\partial x_j} + \frac{\partial \bar{u}_j}{\partial x_i}\right)$, and apparent stress ($\rho u_i' u_j'$) to the fluctuating velocity field.

Menter's SST equation

$$\frac{\gamma}{v_t} P - \beta \rho \omega^2 + \frac{\partial}{\partial x_j}\left[\left(\mu + \sigma_\omega \mu_t\right)\frac{\partial \omega}{\partial x_j}\right] + 2(1 - F_1)2\rho_{\omega 2}\frac{1}{\omega}\frac{\partial k}{\partial x_j}\frac{\partial \omega}{\partial x_j} - \left(\frac{\partial(\rho\omega)}{\partial t} + \frac{\partial\left(\rho u_j \omega\right)}{\partial x_j}\right) = 0 \tag{3}$$

Menter's SST model combines the advantages of the k-ε and k-ω turbulence models in order to provide an effective model formulation that can be used for a wide number of applications. This is

done in order to build an effective model. In order to do this, a blending function known as F1 is introduced. This function has a value of one in the area that is near the solid surface, while it has a value of zero in the flow domain that is farther away from the wall. To be more specific, it causes the k-ε model for residual flow and the k-ω wall area to be triggered. The free stream sensitivity can benefit from the k-ω model's potential in near-wall performance.

2.2 Geometry Modeling

This study used the design shown in Figure 2. The design is indeed based on the concept of ROV, which can be used for underwater exploration and to retrieve small objects. Water Ballast, survey equipment and other essential machinery requires a room of sufficient size. Three-dimensional and two-dimensional views of the ROV's proposed layout are provided. ROV design concept is shown from the side, front, top and in 3-D model (Figure 2(a) until Figure 2(d)). The size details are shown in Table 1

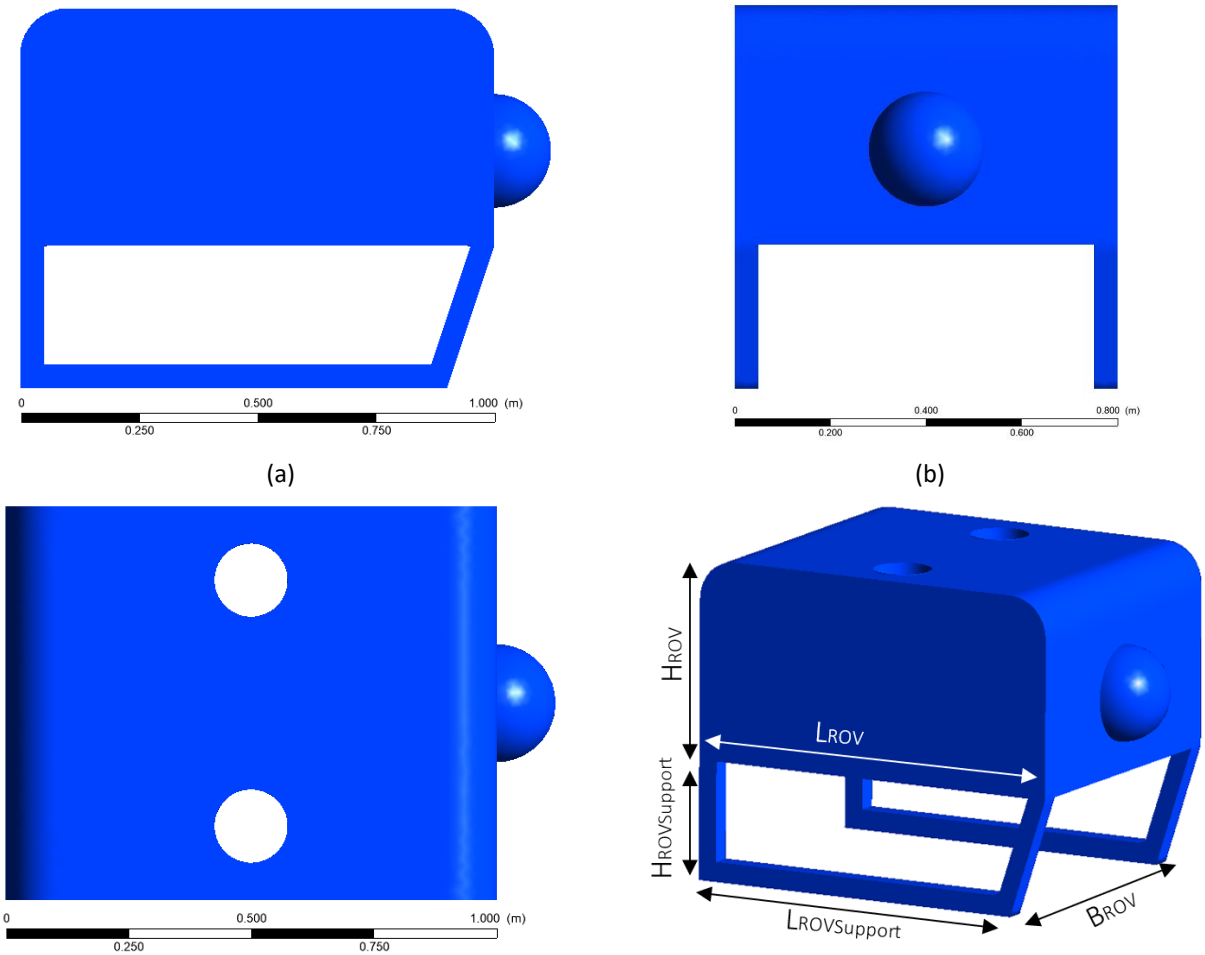

Fig. 2. ROV model (a) Side view (b) Front view (c) Up view (d) ISO view

Table 1
Particular dimension of ROV

	Unit	Dimension
Length (L_{ROV})	m	1
Breadth (B_{ROV})	m	0.8
Heigh (H_{ROV})	m	0.5
Length of Support Platform ($L_{ROVSupport}$)	m	0.9
Heigh ($H_{ROVSupport}$)	m	0.3
Draft ROV at free surface operation	m	0.2
Displacement at free surface operation	kg	160
Displacement at free surface operation	kg	400

2.3 Boundary Condition

ROV is simulated using a CFD approach with calm water conditions and varying depths, namely at the water surface and a depth (h) of 100 m below the water surface. The ROV is conditioned to be in moving at a speed of 0.5 – 1.5 m/s. Preliminary studies assumed the density of the fluid to be the same, namely, 1025 kg/m3. The depth setting and boundary conditions of this simulation are shown in Figure 3. The distance at the front of the hull is up to 3 lengths of the ROV hull model, at the rear of the hull is 5 times the length of the hull. Then the sidewalls are 3 times the model length, and the distance above is 3 times the model length and below 3 times the hull model length. This distance is sufficient enough to avoid the blockage effect [8,16-18].

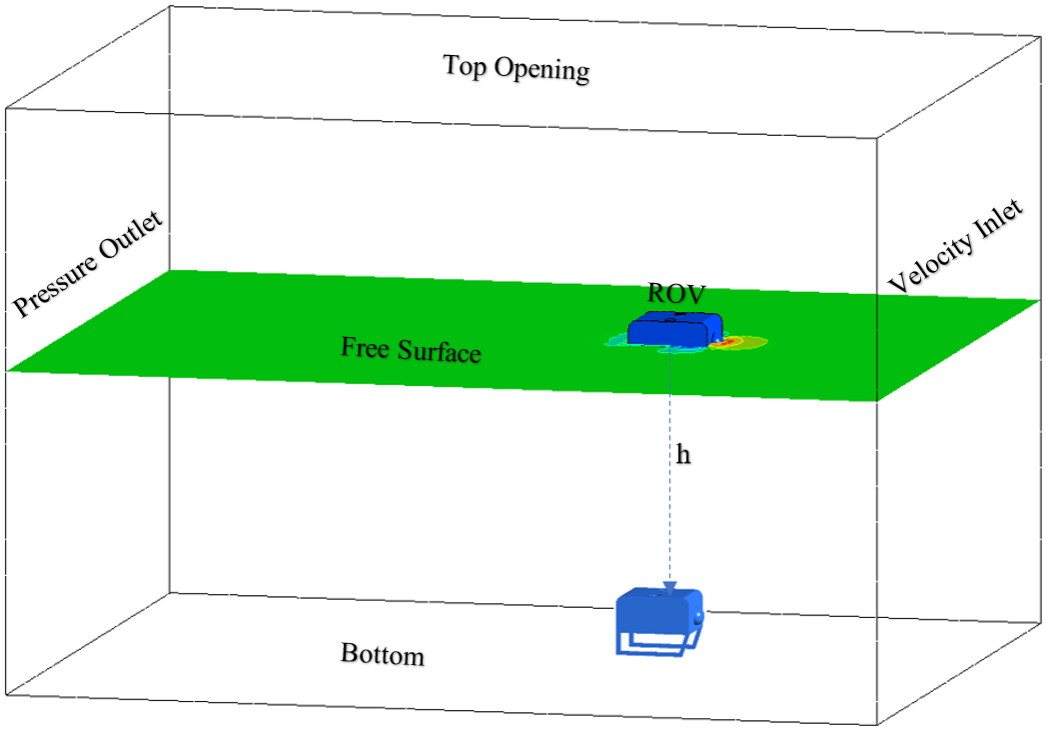

Fig. 3. Boundary condition setting of ROV

2.4 Mesh Generation

The mesh generation method for this study was carried out with the aid of the Design Modeler. A hybrid mesh is a kind of discretization technique whereby the computing area is split between a

structured and unstructured mesh. In order to account for the hull's complex geometry, a triangle-element mesh is built on its surface before the boundary layer is improved using prism elements by extending the surface mesh node. Figure 4 shows how the tetrahedral parts are expanded to cover the whole scene, while a grid is used to make an unstructured mesh that has fewer parts in the far field.

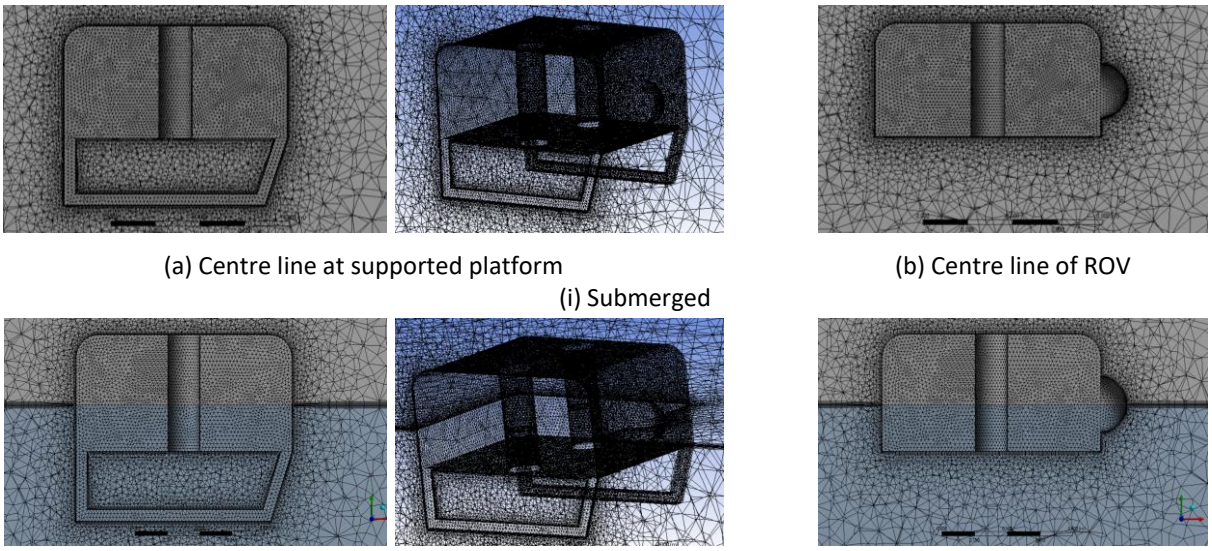

(a) Centre line at supported platform (b) Centre line of ROV

(i) Submerged

(a) Centre line at supported platform (b) Centre line of ROV

(ii) Free surface

Fig. 4. Hybrid mesh of ROV

A higher resolution could always produce excellent outcomes in ANSYS CFX, while at the same time, raising the computational cost and increasing the amount of time it takes because of the large number of elements. The computation procedure takes into account the mesh size in a substantial way. At a velocity of 0.5m/s, mesh convergence tests are carried out for the ROV models in order to determine the mesh size that will offer an acceptable degree of numerical accuracy as well as the total number of elements. The grid independence research is shown in Figure 5. There were about 1.5 million elements for submerged condition and about 1.7 million elements employed for free surface condition.

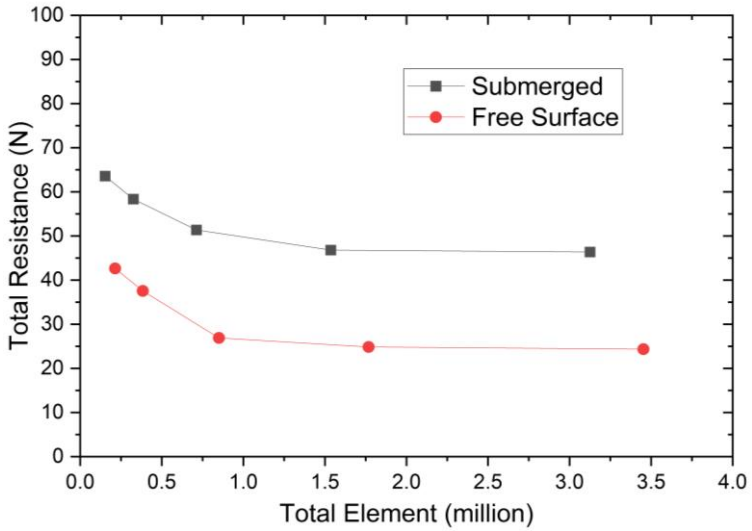

Fig. 5. Grid independence study of ROV

There are a variety of positive outcomes that may result from using a structured mesh in any capacity throughout the development of the grid. The particular sort of mesh layer enables the CFD to properly complete the flow near the wall of the model by describing the flow separation near the hull. This is made possible by the fact that the CFD is able to precisely complete the flow [15]. Figure 6 shows that the right number of mesh layers were chosen to get a value of y+ that was less than 1 on the part of the wall that was close to the ship [19].

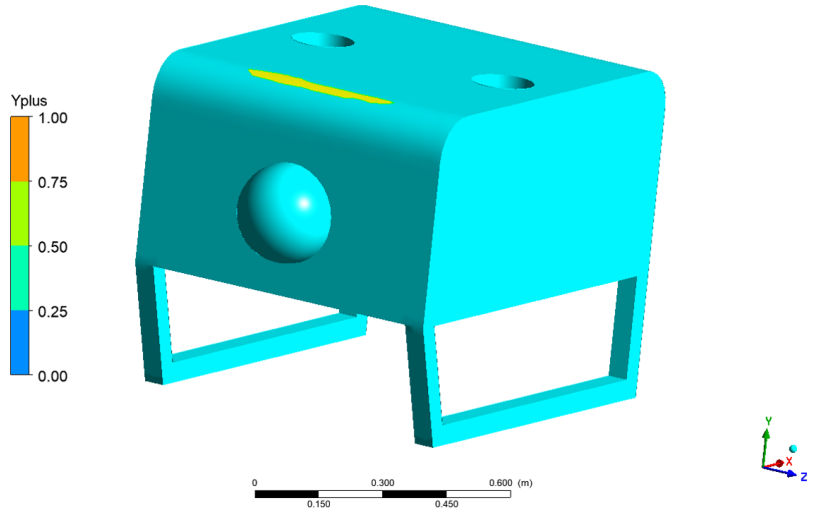

Fig. 6. Y+ value in submerged condition

2.5 *Uncertainty Analysis*

The recommendations made by the ITTC about uncertainty analysis served as the basis for the grid convergence research that was carried out [20]. The convergence investigation was carried out with three distinct mesh resolutions, which were afterwards classified as coarse, medium, and fine, respectively. The mesh was modified by modifying the face size while maintaining the body size with a constant element size. This was done in order to achieve this. Due to the fact that the mesh resolution was determined by the usual wall calculation, the inflation layer was maintained for the entirety of the study, as seen in Table 2.

Table 2
Three varying mesh resolution details of ROV

Model	Detail	Fine (1)	Medium (2)	Coarse (3)
Submerged	Body sizing (m)	0.15	0.15	0.15
	Face sizing (m)	0.015	0.030	0.045
	Number of Elements (NE)	3,124,883	1,535,860	712,466
	Total Resistance (R_T)(N)	46.35	46.79	51.36
Free Surface	Body sizing (m)	0.15	0.15	0.15
	Face sizing (m)	0.015	0.030	0.045
	Number of Elements (NE)	3,452,681	1,786,692	852,245
	Total Resistance (R_T)(N)	24.35	24.84	26.89

The method applies as well to research into other parameters, such as time. Considering that it is high sufficient to be sensitive to parameter changes and low adequate to be utilised to create at least three subsequent solutions while preserving stability, the value $\sqrt{2}$, is suggested for the refinement ratio, ri. The minimum required mesh size is three, however a higher refinement ratio

may be employed if desired. Results have been generated and given in Table 3 based on the formulae in the employed equation section.

Table 3
The uncertainty analysis performed for the ROV

Outcome	Equation	Free Surface	Submerged
Difference of estimation	$\varepsilon_{21}=NE_2/NE_1$	2.2366	2.3479
	$\varepsilon_{32}= NE_3/NE_2$	1.8683	1.8197
Refinement ratio	$r_{21}=R_{T2} -R_{T1}$	0.0002	0.0008
	$r_{32} = R_{T3} -R_{T2}$	0.0008	0.0014
Convergence	$R_i=\varepsilon_{21}/\varepsilon_{32}$	0.2321	0.6018
Order of accuracy	$p=\ln(\varepsilon_{21}/\varepsilon_{32})/\ln(r_i)$	1.8146	0.5949
Extrapolated relative error	$e_{21=} \varepsilon_{21}/r_i^p-1$	0.0000	0.0002
	$e_{32}= \varepsilon_{32}/r_i^p-1$	0.0003	0.0006
Grid convergence index (GCI)	$GCI_{21}=Fs\|e_{21}\|$	0.0000	0.0003
	$GCI_{32=} Fs\|e_{32}\|$	0.0049	0.0510

Prior to evaluating the extrapolated value using the aforementioned equations, the convergence conditions of this system must be established. It is possible to classify the convergence circumstances according to three criteria: The convergence is monotonic for Ri = 0 to 1, oscillatory for Ri<0, and divergent for Ri > 1. Generalized Richardson Extrapolation is used to estimate the error and uncertainty required for monotonic convergence. The oscillations are seen in the data while looking for the convergence of the oscillations. Finally, for divergences, there are divergences of outcomes, but it is difficult to quantify errors and uncertainties.

Grid convergence index, commonly known as GCI, is a standard method for reporting the quality of grid convergence. It is computed at each successive stage in the refining process. As a result, we determined a GCI for the transition from grid 3 to grid 2, as well as the transition from grid 2 to grid 1. where e is the difference in precision between the two grids and Fs is the safety factor (Fs equals 1.25). The resistance was converged based on graphs that demonstrated that the mesh is converged with various mesh fines. This was done in order to simplify the analysis. However, the fine mesh is still selected for the study since it offers more precision to the stimulation and, as a result, reduces the amount of error that is introduced throughout the research.

3. Results

The simulation of ROV resistance at free surface and submerged 100 m underwater show parabolic increase as shown in Figure 7. A sufficiently broad cross-sectional area generates a significant wave impact at the front. As demonstrated in Figure 8, this causes the ROV to encounter greater forward resistance. The wave effect on the water surface caused by the forward motion of the ROV at differing speeds results in different wave height effects at various bow sections. As seen in Figure 8(a), the water level (wave elevation) rises by 0.013 metres. In addition, at a velocity of 0.75 m/s, it creates a wave height increase of 0.27 m, as depicted in Figure 8(b). Furthermore, the wave elevation increased sequentially at a speed of 1 m/s and 1.25 m/s of 0.045 m and 0.070 m, as shown in Figures 8(c) and Figure 8(d). The effect of the highest wave occurrence occurs at a speed variation of 1.5 m/s as shown in Figure 9(e) with a wave height of 0.086m.

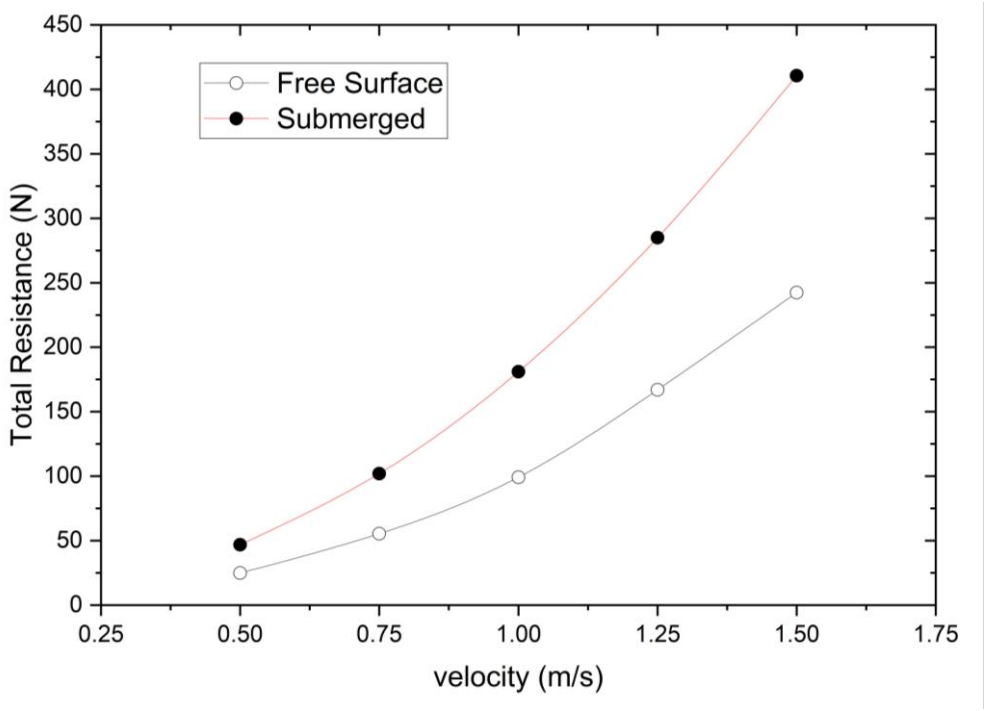

Fig. 7. Resistance of ROV with different condition

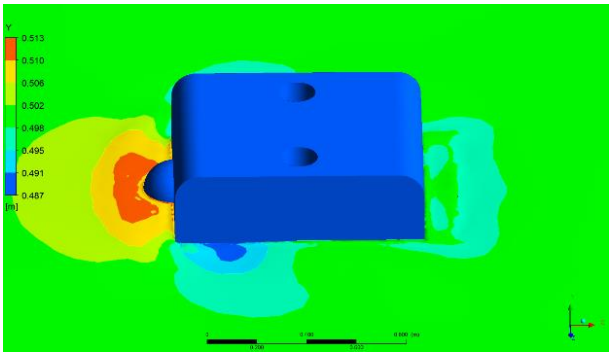

(a)

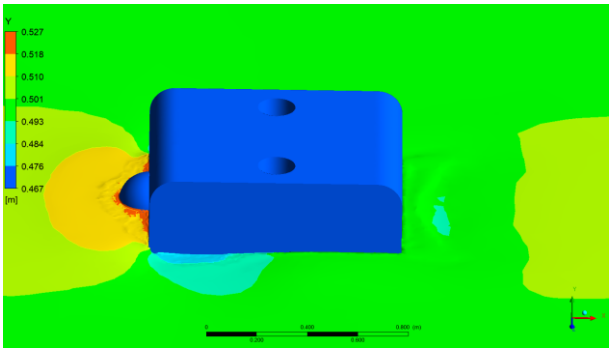

(b)

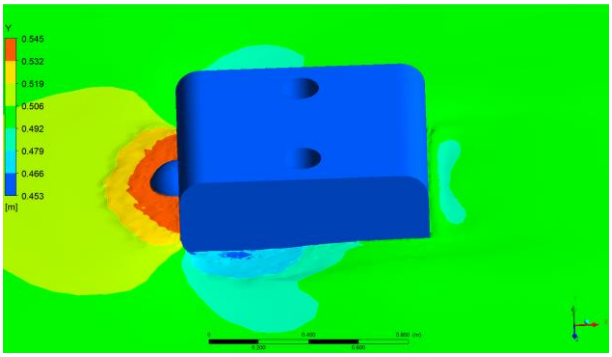

(c)

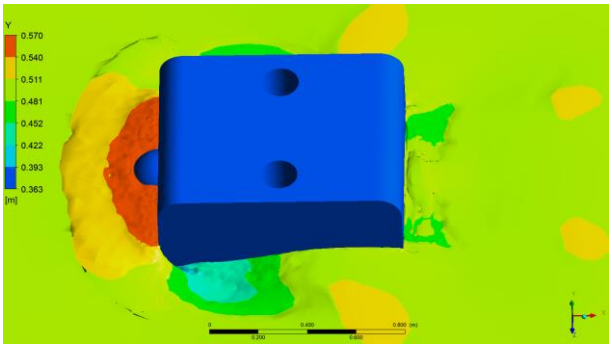

(d)

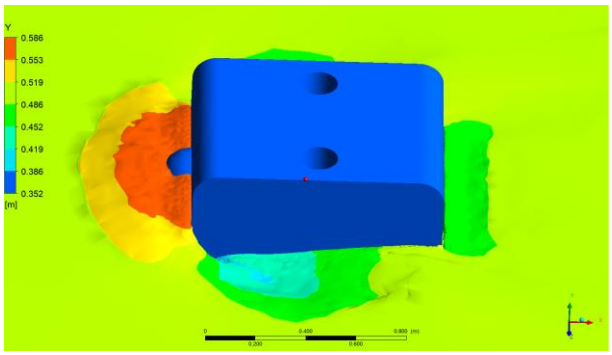

(e)

Fig. 8. Wave elevation at surface condition of ROV with different velocity (a) v = 0.5 m/s (b) v = 0.75 m/s (c) v = 1 m/s (d) v = 1.25 m/s

The increase in resistance occurs due to the phenomenon of turbulence around the ROV hull. The random nature of flow turbulence will significantly increase the resistance. The turbulence flow phenomenon is shown quite well in Figure 9. At low speed (v = 0.5 m/s), the turbulence flow phenomenon is seen significantly at the bottom and rear of the ROV, as shown in Figure 9(a). However, subsequently there was a decrease in the turbulence phenomenon at the bottom of the ROV hull and continued to increase at speeds of 0.75 m/s to moderate 1.25 m/s as shown in Figure 9(b) to Figure 9(d) and then this phenomenon occurred again at speeds 1.5 m/s at the bottom of the ROV as shown in Figure 9(e). The occurrence of this phenomenon causes an increase in inhibition in a parabolic and negative manner.

Figure 9 presents a comprehensive representation of the amount of pressure that exists within the ROV hull. The pressure that rises within the ROV hull has a value of around 972 kPa, which is represented by the red colour on the ROV hull. The absence of a colour shift in the ROV hull in the CFD simulation at different speeds indicates that the pressure inside the ROV hull is not significantly affected by the speed of the ROV. ROV operations on the water surface show a very small total pressure, which is around $1x10^{-3}$ kPa, as shown Figure 10. There is a direct correlation between the depth difference and the amount of pressure change experienced by the ROV's hull. which, the pressure on the ROV hull increases as the depth at which it operates increases.

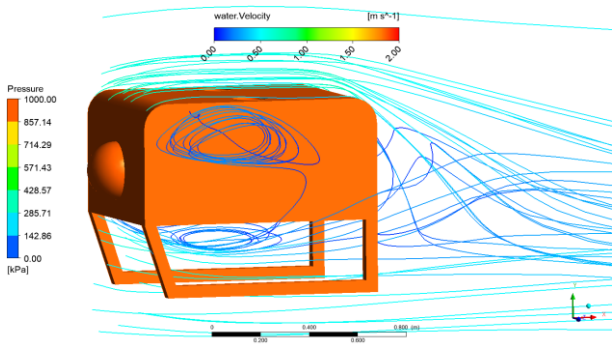

(a)

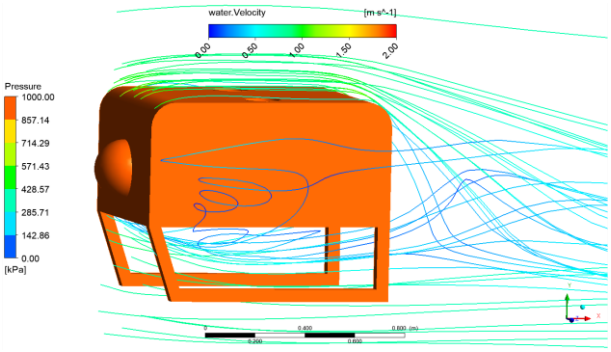

(b)

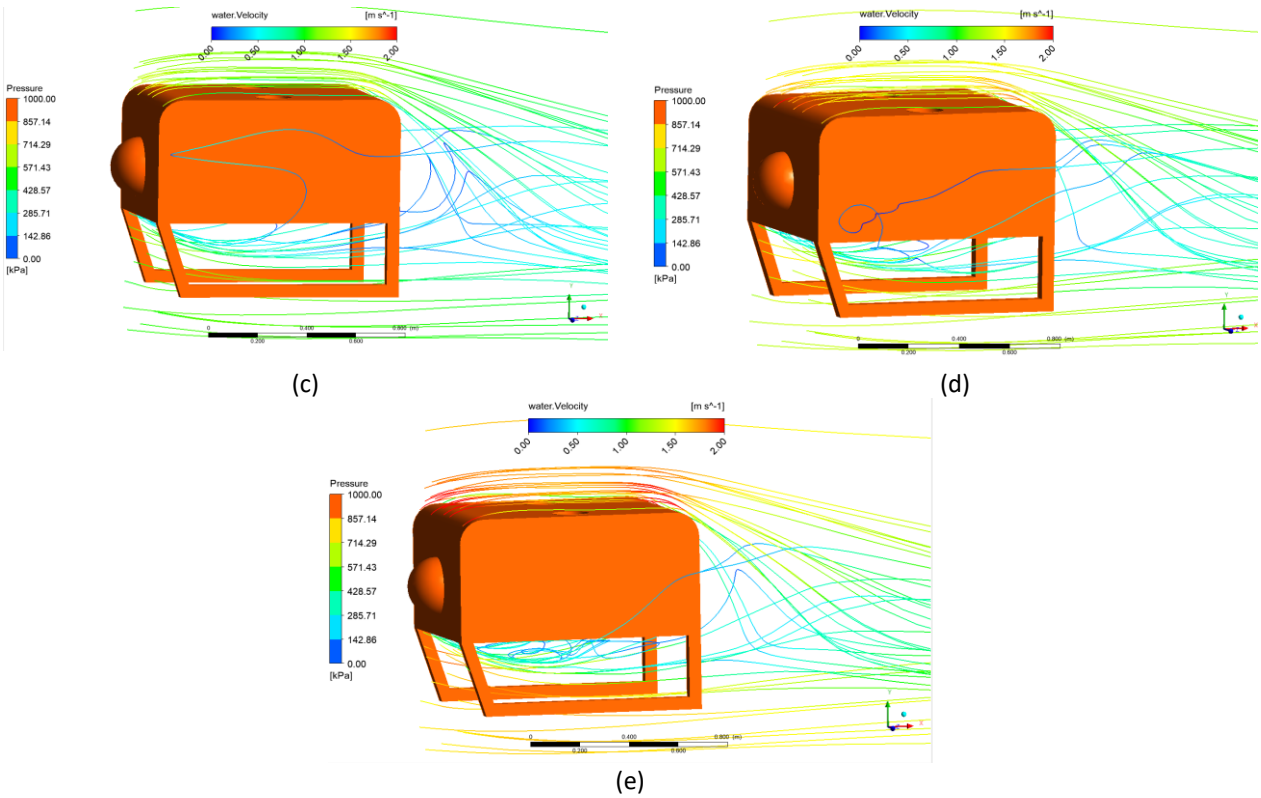

Fig. 9. Pressure dan streamline contour at 100 m underwater of ROV with different velocity (a) v = 0.5 m/s (b) = 0.75 m/s (c) v = 1 m/s (d) v = 1.25 m/s (e) v = 1.5 m /s

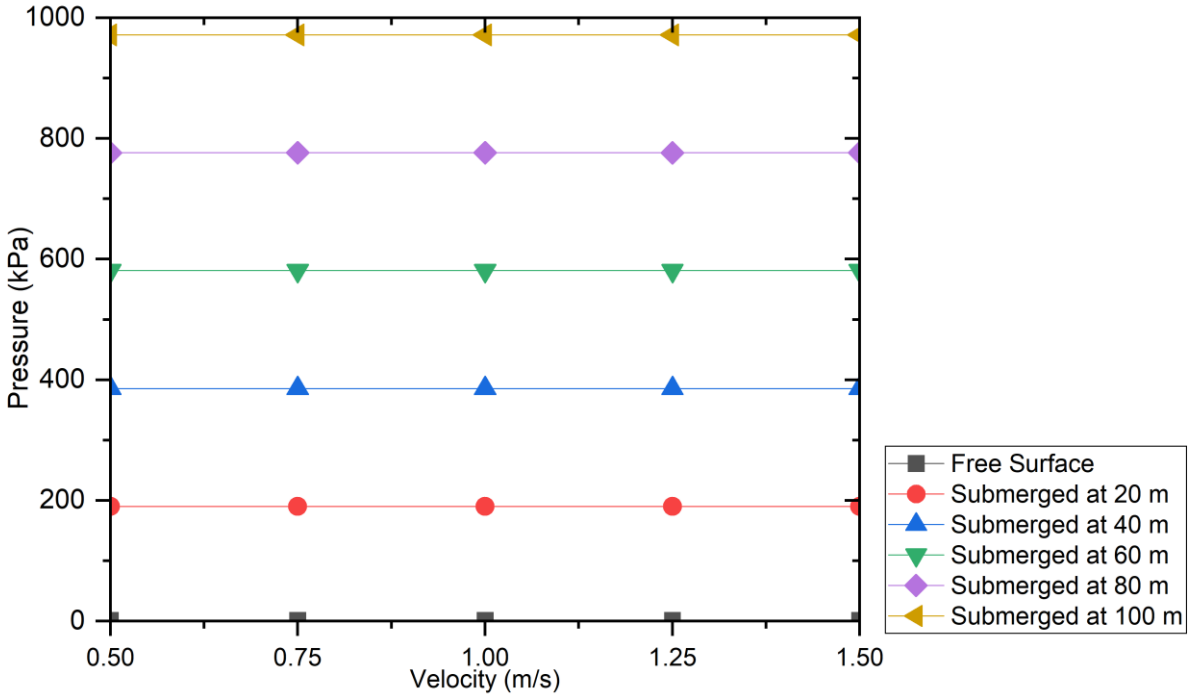

Fig. 10. Total pressure of ROV with different depth

The pressure difference is very small in surface ROV operations, namely an average of 1.11% and 8.2 x 10^{-4}% for submerged operations at a depth of 100 m, as shown in Table 4. The phenomenon that occurs is due to hydrostatic forces due to depth being more dominant than changes in speed.

Thus, the pressure change that occurs in the ROV hull due to velocity is relatively small and, in this case, can be neglected.

Table 4
Percentage difference in ROV pressure with variations in speed and depth

Velocity (m/s)	Free Surface			Submerged at 100 m		
	Pressure (Pa)	Difference (%)		Pressure (Pa)	Difference (%)	
		by velocity	average		by velocity	average
0.5	1.01	-	1,11	971625	-	0.00082
0.75	1.02	0.39		971629	0.00041	
1	1.03	1.28		971632	0.00031	
1.25	1.05	1.84		971643	0.00113	
1.5	1.06	0.94		971657	0.00144	

4. Conclusions

This study explains that CFD makes an excellent contribution regarding the calculation of resistance and pressure on the ROV with conditions on the surface of the water and a depth of 100 m. The ROV simulation produces a significant difference in resistance at a depth of 100m which is about 78.98% greater when compared to the surface condition. Furthermore, the pressure value is not much affected by speed but is significantly affected by the depth of the ROV when operating. ROV simulation results show that the pressure value on the water surface is relatively small, $1x10^{-3}$ kPa, while at a depth of 100m, the pressure value on the ROV hull is 972 kPa.

The pressure change on the ROV's hull is proportional to the depth difference. which increases the pressure on the ROV hull as it operates deeper. The results of this simulation provide a very good picture regarding the pressure value on the ROV hull at that depth, which is very useful for engineers to design ROVs according to the needs related to ROV operational depth.

Acknowledgement
The authors would like to express their gratitude to the Directorate of Research and Community Services (DRPM) Institut Teknologi Sepuluh Nopember for providing financial support under a scheme called flagship research 2022 with contract number: 901/PKS/ITS/2022

References
[1] Xiang, Yan, JinBao Sheng, Lei Wang, YueBo Cai, Ying Meng, and Wei Cai. "Research progresses on equipment technologies used in safety inspection, repair, and reinforcement for deepwater dams." *Science China Technological Sciences* 65, no. 5 (2022): 1059-1071. https://doi.org/10.1007/s11431-021-1958-y

[2] Zhao, Chenyu, Philipp R. Thies, and Lars Johanning. "Offshore inspection mission modelling for an ASV/ROV system." *Ocean Engineering* 259 (2022): 111899. https://doi.org/10.1016/j.oceaneng.2022.111899.

[3] Bonnin-Pascual, Francisco, Alberto Ortiz, Emilio Garcia-Fidalgo, and Joan P. Company-Corcoles. "A reconfigurable framework to turn a MAV into an effective tool for vessel inspection." *Robotics and Computer-Integrated Manufacturing* 56 (2019): 191-211. https://doi.org/10.1016/j.rcim.2018.09.009

[4] Kumar, Saurav, Alireza Mohammadi, David Quintero, Siavash Rezazadeh, Nicholas Gans, and Robert D. Gregg. "Extremum seeking control for model-free auto-tuning of powered prosthetic legs." *IEEE Transactions on Control Systems Technology* 28, no. 6 (2019): 2120-2135. https://doi.org/10.1109/TCST.2019.2928514

[5] Yu, Caoyang, Xianbo Xiang, Philip A. Wilson, and Qin Zhang. "Guidance-error-based robust fuzzy adaptive control for bottom following of a flight-style AUV with saturated actuator dynamics." *IEEE Transactions on Cybernetics* 50, no. 5 (2019): 1887-1899. https://doi.org/10.1109/TCYB.2018.2890582

[6] Christ, R. D. "RLW Sr,“Chapter 3-ROV components,”." *The ROV Manual. Oxford: Butterworth-Heinemann* (2007): 46-80. https://doi.org/10.1016/B978-075068148-3/50007-4

[7] Anuar, Kaspul, and Agung Soegihin. "Aerodynamic Analysis of Unnamed Aerial Vehicle Serindit V-2 Using Computational Fluid Dynamics." *Journal of Advanced Research in Fluid Mechanics and Thermal Sciences* 93, no. 1

(2022): 83-93. https://doi.org/10.37934/arfmts.93.1.8393
[8] ITTC, "Practical Guidelines for Ship CFD Applications," in *27th International Conference Towing Tank*, 2014, vol. 7.5–03 –02, pp. 31 August–5 September. Denmark.
[9] Utama, I. Ketut Aria Pria, and I. K. Suastika. "Experimental and Numerical Investigation into the Effect of the Axe-Bow on the Drag Reduction of a Trimaran Configuration." *International Journal of Technology* 12, no. 3 (2021): 527-538. https://doi.org/10.14716/ijtech.v12i3.4659
[10] Setiawan, Wira, Amalia Ika Wulandari, Aditya Miftahul Huda, and Syerly Klara. "Comparative Study of Ship Resistance and Fuel Consumption between Axe Bow and Moor Deep Ram Bow using CFD Method." *CFD Letters* 14, no. 8 (2022): 71-80. https://doi.org/10.37934/cfdl.14.8.7180
[11] Ansys, C. "Ansys Cfx-Solver Modeling Guide. Canonsburg, PA, USA: ANSYS." (2020).
[12] Menter, Florian R. "Two-equation eddy-viscosity turbulence models for engineering applications." *AIAA journal* 32, no. 8 (1994): 1598-1605. https://doi.org/10.2514/3.12149
[13] Menter, Florian R., Martin Kuntz, and Robin Langtry. "Ten years of industrial experience with the SST turbulence model." *Turbulence, heat and mass transfer* 4, no. 1 (2003): 625-632.
[14] Utama, I. Ketut Aria Pria, Wasis Dwi Aryawan, and Ahmad Nasirudin. "Numerical Investigation into the Pressure and Flow Velocity Distributions of a Slender-Body Catamaran Due to Viscous Interference Effects." *International Journal of Technology* 12, no. 1 (2021): 149-162. https://doi.org/10.14716/ijtech.v12i1.4269
[15] Zeng, Fan-zhi, Jin-ping Li, Yu Wang, Mao Sun, and Chao Yan. "Parametric uncertainty quantification of SST turbulence model for a shock train and pseudo-shock phenomenon." *Acta Astronautica* 196 (2022): 290-302. https://doi.org/10.1016/j.actaastro.2022.05.002.
[16] Elkafas, Ahmed G., Mohamed M. Elgohary, and Akram E. Zeid. "Numerical study on the hydrodynamic drag force of a container ship model." *Alexandria Engineering Journal* 58, no. 3 (2019): 849-859. https://doi.org/10.1016/j.aej.2019.07.004
[17] ITTC, "ITTC – Recommended Procedures and Guidelines: Captive Model Test for Underwater Vehicles," 2021.
[18] Huang, Hai, Zexing Zhou, Hongwei Li, Hao Zhou, and Yang Xu. "The effects of the circulating water tunnel wall and support struts on hydrodynamic coefficients estimation for autonomous underwater vehicles." *International Journal of Naval Architecture and Ocean Engineering* 12 (2020): 1-10. https://doi.org/10.1016/j.ijnaoe.2019.04.008
[19] Procedures, ITTC—Recommended. "Guidelines: Practical guidelines for ship CFD applications." *ITTC Rep* 7 (2014): 2-3.
[20] Procedures, ITTC Recommended. "Uncertainty Analysis in CFD Verification and Validation, Methodology and Procedures." *ITTC Recommended Procedures and Guidelines* (2017): 7-5.